Pinwheel Stabilization by Ocular Dominance Segregation

Lars Reichl,[1,2,*] Siegrid Löwel,[3] and Fred Wolf[1,2]

[1]*Max-Planck-Institute for Dynamics and Self-Organization, Göttingen, Germany*
[2]*Bernstein Center for Computational Neuroscience, Göttingen, Germany*
[3]*Institute of General Zoology and Animal Physiology, University Jena, Jena, Germany*

(Received 25 July 2008; published 18 May 2009)

We present an analytical approach for studying the coupled development of ocular dominance and orientation preference columns. Using this approach we demonstrate that ocular dominance segregation can induce the stabilization and even the production of pinwheels by their crystallization in two types of periodic lattices. Pinwheel crystallization depends on the overall dominance of one eye over the other, a condition that is fulfilled during early cortical development. Increasing the strength of intermap coupling induces a transition from pinwheel-free stripe solutions to intermediate and high pinwheel density states.

DOI: 10.1103/PhysRevLett.102.208101 PACS numbers: 87.19.L−, 05.65.+b, 42.66.Si, 87.19.lp

In the primary visual cortex information is processed in a two-dimensional array of modules called orientation preference (OP) columns [1]. In many species columnar patterns contain pinwheel centers, singular points around which columns activated by different stimulus orientations are radially arranged like the spokes of a wheel [2]. Recent research applying *in vivo* two-photon imaging to pinwheel centers revealed that their radial organization is laid down with single cell precision [3]. How pinwheels are formed during visual development remains unresolved. In theoretical models pinwheels are generated by spontaneous symmetry breaking but are often dynamically unstable [4]. Recent theoretical studies, treating the system of orientation columns essentially as an *isolated* system, have examined if pinwheels may be stabilized by long-range intracortical interactions [5], by a coupling to the large-scale map of visual space [6], or by wiring length constraints [7]. In the visual cortex, however, orientation columns are presumably *interacting* with, e.g., ocular dominance (OD) domains, spatial frequency, and direction preference columns; see, however, [8]. For instance, OD borders intersect many of these preferentially at right angles [9]. It may thus be inadequate to theoretically study the layout of orientation columns neglecting their relation to other columnar systems. Recently this perspective has received experimental support by a study reporting that orientation columns are organized more smoothly when the system of OD columns is removed [10]. Indeed, simulations suggest that OD segregation impedes the process of pinwheel annihilation [4,11]. So far, however, there has been no analytic demonstration that an intrinsically unstable system of orientation pinwheels can be stabilized by interactions with other maps.

Here we present a dynamical systems approach for analyzing the interactions of OP and OD maps. We design a dynamical model for the coordinated development of OP and OD maps in which pinwheels become unstable in the weak coupling limit. The intermap coupling is specified according to experimentally observed geometric relationships between OD and OP maps. Because the contralateral eye dominates during the initial formation of OD columns [12], we systematically study the impact of overall dominance by one eye on the dynamics of pinwheels. Using weakly nonlinear analysis we derive amplitude equations describing the existence and stability of pinwheel-free and pinwheel-rich OP maps in the coupled system. We identify two types of pinwheel-rich solutions differing in their pinwheel density and calculate the stability and phase diagram of these solutions as a function of intermap coupling and contralateral eye dominance. We find that pinwheel crystals are stable above a critical degree of contralateral eye dominance that induces a patchy pattern of OD domains. Increasing the strength of intermap coupling induces a transition from pinwheel-free solutions to low and high pinwheel density patterns. In the latter regime OD segregation even induces the formation of additional pinwheels.

The spatial structure of an OP map is conveniently represented by a complex field $z(\mathbf{x})$ where $\mathbf{x}$ denotes the 2D position of neurons in the visual cortex, the modulus $|z(\mathbf{x})|$ is a measure of their selectivity, and $\theta(\mathbf{x}) = \frac{1}{2}\arg z$ is their preferred orientation [4]. In this representation pinwheel centers are the zeros of the field $z(\mathbf{x})$. Ocular dominance is described by a real field $o(\mathbf{x})$ where negative and positive values indicate ipsilateral and contralateral eye dominance, respectively. Because OD and OP maps are not independent of each other, we consider models containing coupling terms between both fields

$$\begin{aligned} \partial_t z(\mathbf{x}, t) &= F[z(\mathbf{x}, t), o(\mathbf{x}, t)] \\ \partial_t o(\mathbf{x}, t) &= G[z(\mathbf{x}, t), o(\mathbf{x}, t)], \end{aligned} \tag{1}$$

where $F[z, o]$ and $G[z, o]$ are nonlinear operators. Various biologically detailed models have been cast in this form [4,13]. Because cortical maps arise from a cellular instability with a typical wavelength Λ, the mathematically

simplest models for the spontaneous generation of these patterns are of Swift-Hohenberg type [14]. We therefore choose F and G to be of this type and couple the fields through an energy density T

$$\begin{aligned}\partial_t z(\mathbf{x},t) &= L_z z(\mathbf{x},t) - |z|^2 z - \epsilon\frac{\delta T}{\delta \bar{z}}\\ \partial_t o(\mathbf{x},t) &= L_o o(\mathbf{x},t) - o(\mathbf{x},t)^3 + \gamma - \epsilon\frac{\delta T}{\delta o}.\end{aligned} \tag{2}$$

Here $L_{\{o,z\}} = r_{\{o,z\}} - (k_c^2+\Delta)^2$, γ is an OD bias leading to an overrepresentation of the contralateral eye for $\gamma > 0$, and ϵ is the coupling strength. In this model pinwheels are unstable in the weak coupling limit leading to systems of stripes for $\epsilon = 0$, mimicking the behavior of competitive Hebbian models for OD or OP maps in this situation [4]. The form of T is found from the experimental observation that iso-orientation lines tend to intersect the OD borders perpendicularly [9]. T can thus be expected to contain terms of the form $|\nabla o \nabla\theta|^{2m}$. Decomposing the complex field $z(\mathbf{x})$ into the selectivity $|z|$ and the preferred orientation θ finds

$$\begin{aligned}T &= |\nabla z \nabla o|^{2m} = |z|^{2m}(|\nabla o \nabla \ln|z||^2 + 4|\nabla o \nabla\theta|^2)^m\\ &= (|\nabla o \nabla \mathrm{Re} z|^2 + |\nabla o \nabla \mathrm{Im} z|^2)^m.\end{aligned} \tag{3}$$

Where orientation selectivity is locally homogeneous, i.e., $\nabla \ln|z| \approx 0$, T is minimized if the direction of the iso-orientation lines ($\nabla\theta$) is perpendicular to the OD borders. At pinwheel centers the zero contours of $\mathrm{Re} z$ and $\mathrm{Im} z$ cross and $\nabla \mathrm{Re} z$ and $\nabla \mathrm{Im} z$ are not parallel, T can be minimized only if $|\nabla o|$ is small at the pinwheel centers, i.e., near extrema or saddle points of $o(\mathbf{x})$. In the following we analyze the case $m = 2$. As we will see below, this choice allows for a limit in which map interactions become unidirectional.

We observe that for substantial contralateral bias and above a critical coupling ϵ pinwheels are preserved or are even generated after symmetry breaking. Numerical simulations of the dynamics Eq. (2) are shown in Fig. 1. Without a contralateral bias the attractors are pinwheel-free stripe solutions irrespective of the strength of the intermap coupling.

To reveal the exact conditions for the preservation of pinwheels by intermap coupling, we used weakly nonlinear analysis to study the nature and stability of different types of solutions; see [15]. To this end we first studied how the emerging OD map depended on the overall eye dominance. Shifting the OD field by a constant $o(\mathbf{x},t) = \tilde{o}(\mathbf{x},t) + \delta$, the dynamics Eq. (2) is mapped to $\partial_t\tilde{o}(\mathbf{x},t) = \tilde{L}\,\tilde{o} + \tilde{\gamma}\tilde{o}^2 - \tilde{o}^3$ with $\tilde{L} = \tilde{r}_0 - (k_c^2+\Delta)^2$, $\tilde{r}_0 = r_0 - 3\delta^2$, and $\tilde{\gamma} = -3\delta$, where δ is the real solution of $-\delta^3 + (r_0 - k_c)\delta + \gamma = 0$, an equation that has been extensively studied in pattern formation literature [16]. It has three types of stationary solutions: (1) a homogeneous solution with spatially constant eye dominance $o_c(\mathbf{x}) = \delta$, (2) OD stripes $o_{\mathrm{st}}(\mathbf{x}) = 2\mathcal{B}_{\mathrm{st}}\cos(x+\psi) + \delta$, with $\mathcal{B}_{\mathrm{st}} = \sqrt{\tilde{r}/3}$, and (3) hexagonal arrays of ipsilateral eye dominance blobs in a sea of contralateral eye dominance $o_{\mathrm{hex}}(\mathbf{x}) = \mathcal{B}_{\mathrm{hex}}\sum_{j=1}^3 e^{\imath\psi_j}e^{\imath\vec{k}_j\vec{x}} + \mathrm{c.c.} + \delta$, with $\sum_j^3 \vec{k}_j = 0$, $\sum_j^3 \psi_j = \pi$, and $\mathcal{B}_{\mathrm{hex}} = -\tilde{\gamma}/15 + \sqrt{(\tilde{\gamma}/15)^2 + \tilde{r}/15}$. The fractions of contralateral eye dominated territory C_{st} and C_{hex} increase with γ as $\cos(C_{\mathrm{st}}\pi) = -\delta/(2\mathcal{B}_{\mathrm{st}})$ and $(1-C_{\mathrm{hex}})\times\sqrt{3}2\pi \approx 3\arccos[\frac{1}{2}(-1+\sqrt{3+\frac{\delta}{\mathcal{B}_{\mathrm{hex}}}})]^2$ for (2) or (3) [Fig. 2(b)]. The phase diagram of this model is depicted in Fig. 2(a). It shows the stability borders for the three solutions. Without a bias term the OD map is either constant, for $r_0 < 0$, or has a stripe layout, for $r_0 > 0$. For positive r_0 and increasing bias term there are two transition regions. First, a transition region from stripes to hexagons (between γ^* and γ_2^*) and, second, a transition region from hexagons to the homogeneous solution (between γ_3^* and γ_4^*).

Close to instability, stationary solutions to the full dynamics Eq. (2) can be calculated analytically by weakly nonlinear analysis [17]. The Fourier components of the emerging pattern are located on the critical circle $\vec{k}_j = (\cos j\pi/3, \sin j\pi/3)k_c$ so that

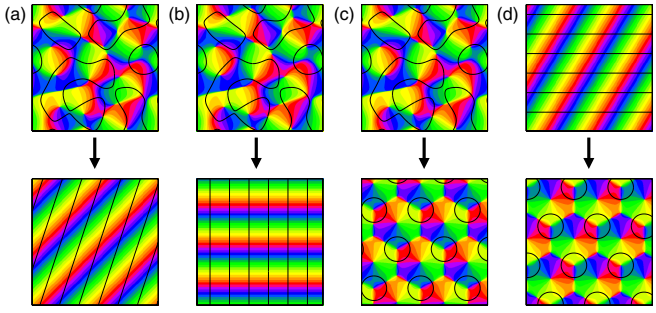

FIG. 1 (color online). Pinwheel annihilation and preservation in simulations of Eq. (2) for different strengths of intermap coupling and OD bias, $r_0 = 0.2$, $r_z = 0.02$. Color-coded OP map, zero contours of OD map superimposed. (a),(b) $\gamma = 0$, $\epsilon = 0, 2000$ (c),(d) $\gamma = 0.15$, $\epsilon = 2000$. Upper (lower) row: $t = 0$ $(10^4/r_z)$. Initial conditions identical in (a)–(c).

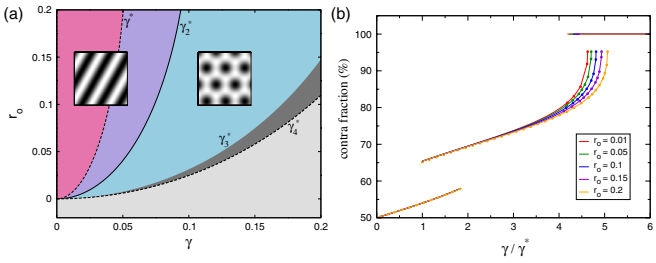

FIG. 2 (color online). (a) Phase diagram of the OD model Eq. (2). Dashed lines: Stability border of hexagon solutions; solid line: stability border of stripe solution; gray regions: stability region of homogeneous solution. (b) Contralateral eye dominated neurons for the three stationary solutions. Circles: Numerically obtained values; solid lines: C_{st} and C_{hex}.

$$z(\mathbf{x},t)=\sum_j^3 (A_j(t)e^{\imath\vec{k}_j\vec{x}}+A_{j^-}(t)e^{-\imath\vec{k}_j\vec{x}})$$
$$o(\mathbf{x},t)=\sum_j^3 (B_j(t)e^{\imath\vec{k}_j\vec{x}}+\bar{B}_j(t)e^{-\imath\vec{k}_j\vec{x}}), \quad (4)$$

with the complex amplitudes $A_j=\mathcal{A}_j e^{\imath\phi_j}$, $B_j=\mathcal{B}_j e^{\imath\psi_j}$. Although the coupling terms enter at seventh order in the amplitude expansion, they can be written as an effective cubic interaction term. Because $A_i\propto\sqrt{r_z}$ and $B_i\propto\sqrt{r_0}$, the coupling onto the OD dynamics becomes small for $r_z\ll r_0$, since terms like $\epsilon|A|^4|B|^2B\propto r_z^2 r_0^{3/2}$ are negligible compared to terms like $|B|^2B\propto r_0^{3/2}$. In this limit, the backreaction of the OP map onto the OD map is thus negligible. Using uniform modes $\mathcal{B}_i=\mathcal{B}$, the amplitude equations for the OP map are given by

$$\partial_t A_i = r_z A_i-\sum_j^6 g_{ij}|A_j|^2A_i-2\sum_{j\neq i}^3 A_jA_{j^-}\bar{A}_{i^-}$$
$$-\epsilon\mathcal{B}^4\sum_{j,l,k}^6 h_{ijlk}A_jA_l\bar{A}_k, \quad (5)$$

with $A_{j^-}=A_{j+3}$, $g_{ii}=1$, $g_{ij}=2$, and h_{ijlk} an effective self-interaction tensor. The dynamics of the modes A_{i^-} is given by interchanging A_i and A_{i^-}. A solution of hexagonal symmetry (symmetric under rotation by 120°) to Eq. (5) is given by the uniform solution $\mathcal{A}_j=\mathcal{A}_{j^-}=\mathcal{A}$, $\phi_j=\psi_j+(j-1)2\pi/3+d\delta_{j,2}$, and $\phi_{j^-}=-\psi_j+(j-1)2\pi/3+d(\delta_{j,1}+\delta_{j,3})$, where we choose $\psi_1=\psi_3=0$, $\psi_2=\pi$, and the constant $d\approx 1.176$ is the solution of a transcendental equation. For negligible backreaction $\mathcal{B}=\mathcal{B}_{\mathrm{hex}}$ and $\mathcal{A}^2\approx r_z/(9+55.6\epsilon\mathcal{B}_{\mathrm{hex}}^4)$. The uniform solution is determined up to a free phase φ which results from the orientation shift symmetry $z\rightarrow ze^{\imath\varphi}$ of Eq. (2). The positions of the pinwheels are fixed by the OD map and there are no translational degrees of freedom. In addition to these hexagonal pinwheel crystals (HPWCs) there exist also nonuniform solutions. In addition to stripelike solutions of $z(\mathbf{x})$ with one dominant mode we find rhombic pinwheel crystals (RPWCs) $\mathcal{A}_j=\mathcal{A}_{j^-}=(\mathcal{A},a,\mathcal{A})$ with $a\ll\mathcal{A}$ and distorted rhombic crystals $\mathcal{A}_j=(\mathcal{A}_1,\mathcal{A}_2,\mathcal{A}_3)$, $A_{j^-}=(\mathcal{A}_3,\mathcal{A}_2,\mathcal{A}_1)$, both symmetric under rotation by 180°. We analytically calculated the stability properties of the uniform solution by linear stability analysis. The phase diagram for $r_z\ll r_0$, cf. Fig. 3(a), reveals a transition from RPWCs to HPWCs with increasing coupling strength ϵ for intermediate degrees of OD bias. For $\gamma<\gamma^*$ or for $\gamma>\gamma_4^*$ pinwheel-free orientation stripes are dynamically selected. For $\gamma^*<\gamma<\gamma_4^*$ and above a critical effective coupling strength $\epsilon\mathcal{B}^4\approx 0.042$, HPWCs are stable and become the energetic ground state above $\epsilon\mathcal{B}^4\approx 0.12$. Below $\epsilon\mathcal{B}^4\approx 0.065$, RPWCs are stable leading to a bistability region between RPWCs and HPWCs. We find in this region that RPWCs transform into distorted RPWCs above an effective coupling strength of $\epsilon\mathcal{B}^4\approx 0.033$. Although RPWCs are stable even in the uncoupled case, they never become the energetic ground state. Thus for substantial bias towards one eye pinwheels are in fact stabilized and pinwheel-rich solutions become ground states by intermap coupling.

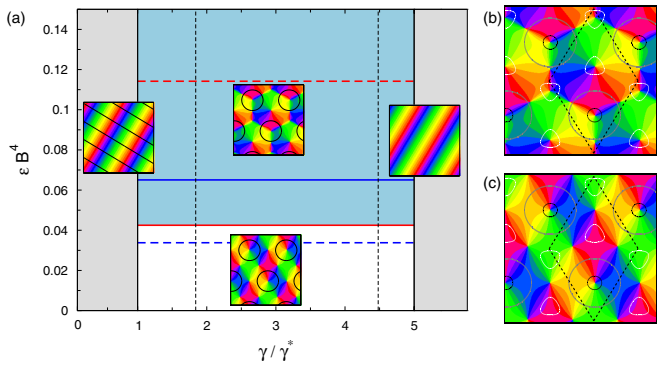

FIG. 3 (color online). (a) Phase diagram of the model Eq. (5) for $r_z\ll r_0$. Vertical lines: Stability range of OD hexagons; lower solid line: stability border of HPWC; upper solid line: stability border of RPWC; lower dashed line: transition from rhombic to distorted RPWC. HPWC is ground state above the upper dashed line. (b) HPWC, (c) RPWC. OD contour lines: 10%, 50%, 90% contralateral eye dominance (black, gray, white); dashed line: unit cell.

The layouts of the main pinwheel-rich solutions are shown in Figs. 3(b) and 3(c). The HPWC contains six pinwheels per unit cell and the pinwheel density, i.e., the number of pinwheels per Λ^2 [4], is given by $\rho=6\cos(\pi/6)\approx 5.2$. The RPWC has four pinwheels per unit cell and its pinwheel density is $\rho=4\cos(\pi/6)\approx 3.5$. One may expect that the energy term Eq. (3) favors pinwheels to colocalize with OD extrema. For HPWCs three pinwheels of the same topological charge are in fact located at the extrema of the OD map. The other three, however, are located near OD borders. In case of the rhombic layout there is only one pinwheel at an OD extremum while the other three pinwheels are located at OD saddle points which are also energetically favorable positions with respect to T.

We tested whether these solutions and their stability ranges revealed for $r_z\ll r_0$ persist when the backreaction on the OD map is taken into account. To this end we solved the full field dynamics Eq. (2) numerically using a fully implicit Krylov subspace algorithm with periodic boundary conditions on a 128×128 mesh with an aspect ratio of $\Gamma=22$. In simulations we tracked the pinwheel density from $t=0$ to $t=10^4 r_z^{-1}$, cf. Fig. 4. In the uncoupled case ($\epsilon=0$), most of the patterns decay into a stripe solution and their pinwheel density drops towards zero. At small coupling strengths ($\epsilon=200$) the pinwheel density converges either to zero (stripes), to values near 3.5 for the RPWC, or to approximately 5.2 for the HPWC. At high map coupling ($\epsilon=2000$), pinwheel-free stripe patterns form neither from pinwheel-rich nor from pinwheel-free

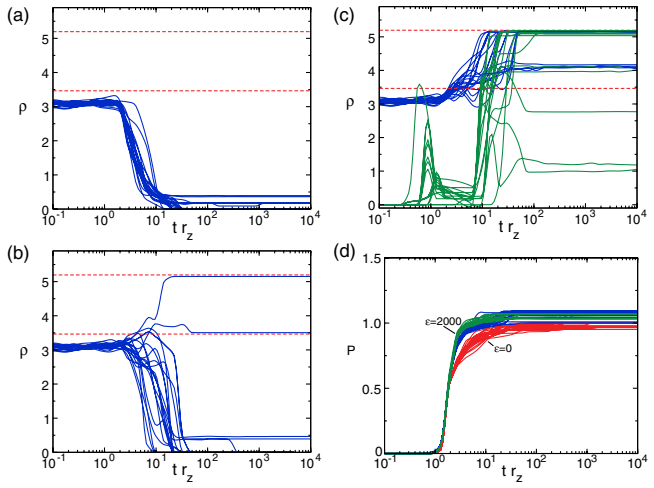

FIG. 4 (color online). Time evolution of the pinwheel density for $r_z = 0.05$, $r_0 = 0.25$, $\gamma = 0.15$. (a)–(c) Simulations started from an identical set of 20 initial conditions. Dashed lines: $\rho = 4\cos(\pi/6)$ and $\rho = 6\cos(\pi/6)$. (a)–(c) $\epsilon = 0, 200, 2000$. (c) OD and OP stripes as initial conditions [light gray (green) lines]. (d) Power of OP map, $\epsilon = 0, 200, 2000$ (red lines, blue lines, green lines).

initial conditions. In this regime the dominant layout is the HPWC. However, regions of HPWC layout can be interdigitated with long-lived RPWCs and stripe domains. Figure 4(d) shows the time course of the power $P(t) = \langle |z(\mathbf{x}, t)_{\mathrm{dyn}}|^2 \rangle_{\mathbf{x}} / \langle |z(\mathbf{x}, t)_{\mathrm{th}}|^2 \rangle_{\mathbf{x}}$. The field z_{th} is obtained from solution of the amplitude equations Eq. (4) while z_{dyn} is the field obtained from the simulation. The amplitudes grow and saturate after $t \approx r_z^{-1}$. When the amplitudes are saturated, pattern selection starts. Quantitatively, we find that with backreaction the critical coupling strengths are slightly increased compared to their values in the limit $r_z \ll r_0$.

Our analysis for the first time conclusively demonstrates that OD segregation can stabilize pinwheels, even if they are intrinsically unstable in the uncoupled dynamics of the OP map, raising the possibility that intermap coupling is the mechanism of pinwheel stabilization in the visual cortex. Our results indicate that the overall dominance of one eye is important for the effectiveness of this mechanism. In this case, OD domains form a system of patches rather than stripes enabling the capture and stabilization of pinwheels by intermap coupling. Studying a wide range of phenomenologically conceivable interaction energies we find that systems of OD stripes are in general not expected to stabilize pinwheel patterns. Interestingly, visual cortex around the time of early OP development is indeed dominated by one eye and has a pronounced patchy layout of OD domains supporting this notion [12]. Further support comes from experiments in which the OD map was removed artificially, resulting in a significantly smoother OP map [10]. Removal of the OD map, however, apparently does not completely destabilize pinwheels. This might reflect the influence of additional columnar systems of patchy layout like spatial frequency or direction columns that are expected to interact with the OP map in a similar fashion as OD columns. Interactions among multiple coupled maps may potentially also explain the noncrystalline spatial organization of OP maps in the visual cortex. The approach introduced here will be useful for further rigorous analyses of the interaction among multiple maps in cortical development.

We thank D. Heide and M. Kaschube for providing the Krylov algorithm and for fruitful discussions. We thank M. Huang for discussions. This work was supported by the HFSP and BMBF.

*reichl@nld.ds.mpg.de

[1] D. H. Hubel and T. N. Wiesel, Proc. R. Soc. London **198**, 1 (1977).
[2] A. Grinwald *et al.*, Nature (London) **324**, 361 (1986); G. G. Blasdel and G. Salama, Nature (London) **321**, 579 (1986); N. Swindale, J. Matsubara, and M. Cynader, J. Neurosci. **7**, 1414 (1987); T. Bonhoeffer and A. Grinwald, Nature (London) **353**, 429 (1991); B. Chapman, M. P. Stryker, and T. Bonhoeffer, J. Neurosci. **16**, 6443 (1996); W. H. Bosking *et al.*, J. Neurosci. **17**, 2112 (1997).
[3] K. Ohki *et al.*, Nature (London) **442**, 925 (2006); J. Schummers, H. Yu, and M. Sur, Science **320**, 1638 (2008).
[4] F. Wolf and T. Geisel, Nature (London) **395**, 73 (1998).
[5] F. Wolf, Phys. Rev. Lett. **95**, 208701 (2005); M. Kaschube, M. Schnabel, and F. Wolf, New J. Phys. **10**, 015009 (2008).
[6] N. Mayer, M. J. Herrmann, and T. Geisel, Neurocomputing **38–40**, 279 (2001); H. Y. Lee, M. Yahyanejad, and M. Kardar, Proc. Natl. Acad. Sci. U.S.A. **100**, 16 036 (2003); P. J. Thomas and J. D. Cowan, Phys. Rev. Lett. **92** 188101, (2004).
[7] A. Koulakov and D. Chklovskii, Neuron **29**, 519 (2001).
[8] A. Basole, L. E. White, D. Fitzpatrick, Nature (London) **423**, 986 (2003).
[9] E. Bartfeld and A. Grinwald, Proc. Natl. Acad. Sci. U.S.A. **89**, 11 905 (1992); K. Obermayer and G. G. Blasdel, J. Neurosci. **13**, 4114 (1993); M. C. Crair *et al.*, J. Neurophysiol. **77**, 3381 (1997); M. Hübener *et al.*, J. Neurosci. **17**, 9270 (1997); S. Löwel *et al.*, Eur. J. Neurosci. **10**, 2629 (1998).
[10] B. Farley *et al.*, J. Neurosci. **27**, 10 299 (2007).
[11] M. W. Cho and S. Kim, Phys. Rev. Lett. **92** 018101, (2004); D. M. Pierre, Master's thesis, MIT, 1997.
[12] M. C. Crair, D. C. Gillespie, and M. P. Stryker, Science **279**, 566 (1998); N. P. Issa *et al.*, J. Neurosci. **19**, 6965 (1999).
[13] F. Wolf *et al.*, J. Physiol. (Paris) **94**, 525 (2000).
[14] M. C. Cross and P. C. Hohenberg, Rev. Mod. Phys. **65**, 851 (1993).
[15] See EPAPS Document No. E-PRLTAO-102-009923 for supplementary material. For more information on EPAPS, see http://www.aip.org/pubservs/epaps.html.
[16] A. Soward, Physica (Amsterdam) **14D**, 227 (1985).
[17] P. Mannevile, *Dissipative Structures and Weak Turbulence* (Academic, New York, 1990).